

# 27th International Symposium on Space Flight Dynamics 2019 (ISSFD)

*Please select category below:*

Normal Paper

Student Paper

Young Engineer Paper

## Drag-Free and Attitude Control System in LEO using Cold Gas Propulsion System: a feedback from the MICROSCOPE mission

S. Delavault <sup>1</sup>, P. Prieur <sup>1</sup>, T. Liénart <sup>1</sup>, J. Moyard <sup>1</sup>, A. Robert <sup>1</sup>, V. Cipolla <sup>1</sup>, PY. Guidotti <sup>1</sup>

<sup>1</sup> Centre national d'Etudes Spatiales, Toulouse, France

### Abstract

Microscope is a CNES-ESA-ONERA-CNRS-OCA-DLR-ZARM mission dedicated to the test of the Equivalence Principle with an improved accuracy of  $10^{-15}$ . The 300kg drag-free microsatellite was launched on April 25<sup>th</sup> 2016 into a 710km dawn-dusk sun-synchronous orbit. It has been de-orbited on October 16<sup>th</sup> 2018.

To comply with stringent scientific requirements, the Drag Free and Attitude Control System involves the scientific accelerometer as main sensor and a Cold Gas Propulsion System composed of 8 proportional micro-thrusters as main actuator.

After a successful 2-year mission, the paper draws a feedback of the use of the CGPS in a DFACS point of view: dimensioning process of the CGPS architecture, in-flight performance and results of end-of life experiments will be detailed.

**Keywords:** Microscope, DFACS, CGPS

### Introduction

Microscope is a CNES-ESA-ONERA-CNRS-OCA-DLR-ZARM mission dedicated to the in-orbit test of the Equivalence Principle of Einstein's general relativity theory with an improved accuracy of  $10^{-15}$ . The idea is to observe the free-fall motion of masses made of different materials using the Earth as a gravitational source.

The 300kg drag-free microsatellite was launched on April 25<sup>th</sup> 2016 into a 710km dawn-dusk sun-synchronous orbit. It has been de-orbited on October 16<sup>th</sup> 2018.

To comply with stringent scientific requirements, the Drag Free and Attitude Control System (DFACS) involves the scientific accelerometer as main sensor and a Cold Gas Propulsion System (CGPS) composed of 8 proportional micro-thrusters (MT) as main actuator.

After a successful 2-year mission, the paper draws a feedback of the use of the CGPS within the DFACS.

After a brief description of the Microscope mission, we will describe the dimensioning process of the CGPS architecture: historical background leading to the use of a CGPS for drag-free and attitude control; architectural choices such as the number, position and orientation of the

thrusters; and gas consumption studies performed to determine the critical parameters impacting the mission life-time.

Then, in-flight performance will be detailed, such as the gas consumption monitoring. In addition to the short term monitoring, the estimation of the consumption for each type of guidance was used to foresee the evolution of the gas capacity depending on the mission scenario. We will see how the attitude guidance impacts the perturbation torques and finally the gas consumption, typically from 1 gram per orbit to 6 grams per orbit. These observations led to take into account carefully the gas capacity prediction in the update process of the mission scenario.

After the end of the scientific mission, some end-of life experiments were conducted, leading to a better characterization of the propulsion system. Results of thrust calibrations or test of the redundant configuration will be detailed.

Finally, we will focus on collision avoidance, performed with the CGPS, and de-orbiting, for which an innovative solution has been implemented to increase drag.

To conclude, in the “Lessons Learned” section, we will present possible solutions to save some gas.

## **Microscope Mission**

### **Mission’s Scientific Objective**

Since Galilee, we know that two bodies released in the vacuum, with the same initial conditions, touch the floor simultaneously, whatever their mass. This concept has been conceptualized in the Equivalent Principle (EP) by Albert Einstein, and is the basis of his theory of general relativity.

The mission's main scientific objective is the test of the universality of free-fall, with an accuracy of  $10^{-15}$  i.e. more than a 100 times better than the accuracy of the present ground experiments.

The results of this experiment will be a major event in fundamental physics. A violation of the EP would lead to the evidence of a new atomic interaction which is predicted by current quantum theories of gravity. On the opposite, if the EP is verified, the theories assuming a violation of the EP at this level of magnitude could be discarded or at least very constrained.

### **Experiment principle**

The EP postulates the equivalence between the inertial mass and the gravitational mass. A well-known consequence of this principle is that two objects submitted only to the same gravitational field have exactly the same acceleration, regardless of their composition. For the MICROSCOPE experiment, the Earth is the gravitational source and two test-masses of different compositions are observed in free-fall condition.

The high accuracy acceleration measurements were performed by a differential electrostatic accelerometer developed by ONERA, called SAGE (Space Accelerometer for Gravity Experiment). SAGE is composed of two concentric, coaxial, cylindrical test masses (TM) with a common center of gravity suspended in a highly stable electrode cage. The external TM is made of titanium and the internal of platinum-rhodium.

The principle of operation is to measure the electrostatic forces required from the electrodes to maintain the relative position of the test masses (TM) in the cage. Since both electrode cages

experience the same acceleration, the differential measurement is the difference between the gravitational acceleration of the two masses:

$$\vec{S} = \vec{\gamma}_1 - \vec{\gamma}_2 = \delta \times \vec{g} \quad \text{Eq. 1}$$

where  $\vec{g}$  is the Earth gravitational acceleration (7.8 m/s<sup>2</sup> at 700 km of altitude) and  $\delta$  is the equivalence principle violation parameter (Eötvös parameter, cf. Eq. 2) that must be identified with an accuracy of 10<sup>-15</sup>. In particular, that means that  $(\vec{\gamma}_1 - \vec{\gamma}_2)$  must be measured with accuracy below 7,5.10<sup>-15</sup> m/s<sup>2</sup>.

$$\delta = \left( \frac{m_{1g}}{m_{1i}} - \frac{m_{2g}}{m_{2i}} \right) \quad \text{Eq. 2}$$

In order to confirm the experimental process and the measurement accuracy, a second SAGE with two TM made with the same material (platinum-rhodium) is installed on-board (TSAGE: Twin Space Accelerometer for Gravity Experiment).

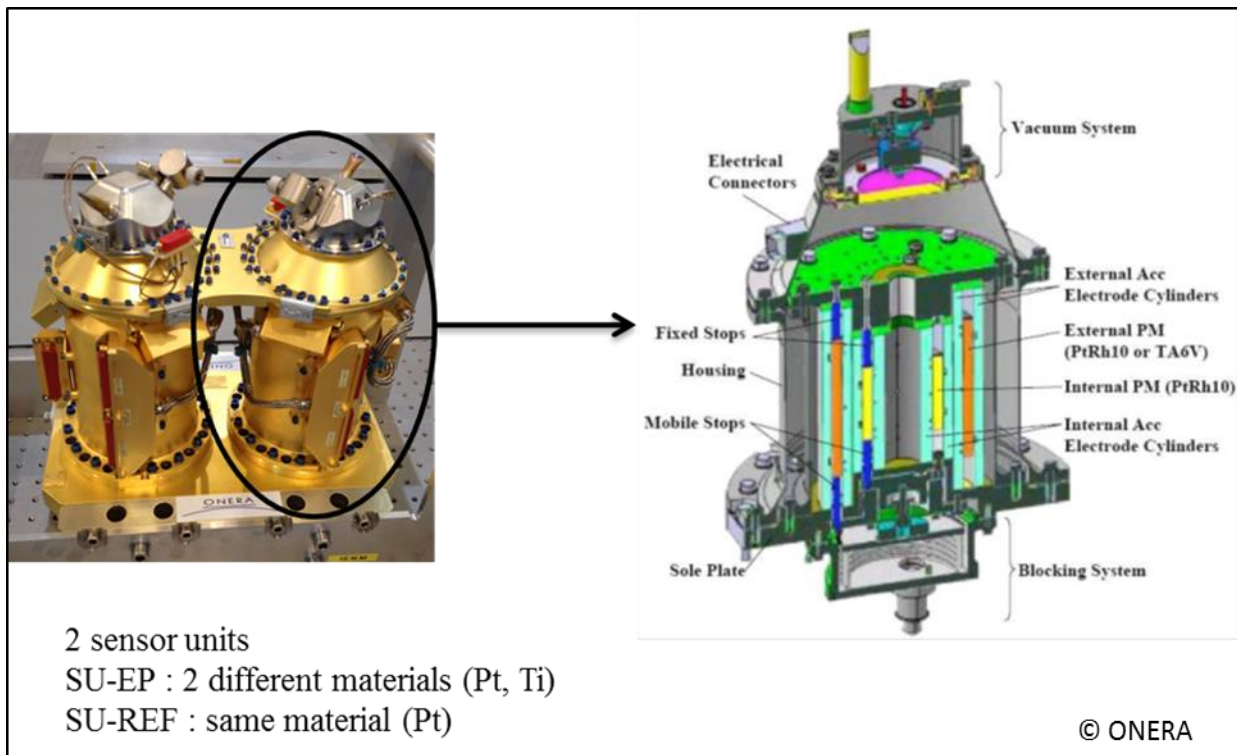


Figure 1 TSAGE : Twin Space Accelerometer for Gravity Experiment

### Mission Description: Orbit and Pointing

MICROSCOPE flew on a dawn-dusk sun synchronous orbit at 710 km of altitude. The EP measurements were carried-out during different types of measurement sessions:

#### Inertial Sessions

In the mission design, inertial sessions of 8 days were defined. In these sessions, the satellite is inertially pointed (i.e. it just follows the one degree per day drift of the orbital plane). The main axis of the accelerometer ( $X_{inst} \sim Z_{sat}$ ) is in the orbital plane. The EP hypothetical violation signal is expected to be a sine at the rotational frequency of the  $g$  in satellite frame  $f_{ep} = f_{orb} \approx 0.168$  mHz.

But after the in-flight testing phase, it appeared that these sessions were not useful to assess the required performance. Indeed, the acceleration measurements showed a high level of stochastic noise for low frequencies (including  $F_{orb}$ ) incompatible with the required performance. Thus these sessions were deprogrammed from the mission scenario in order to work at higher frequencies.

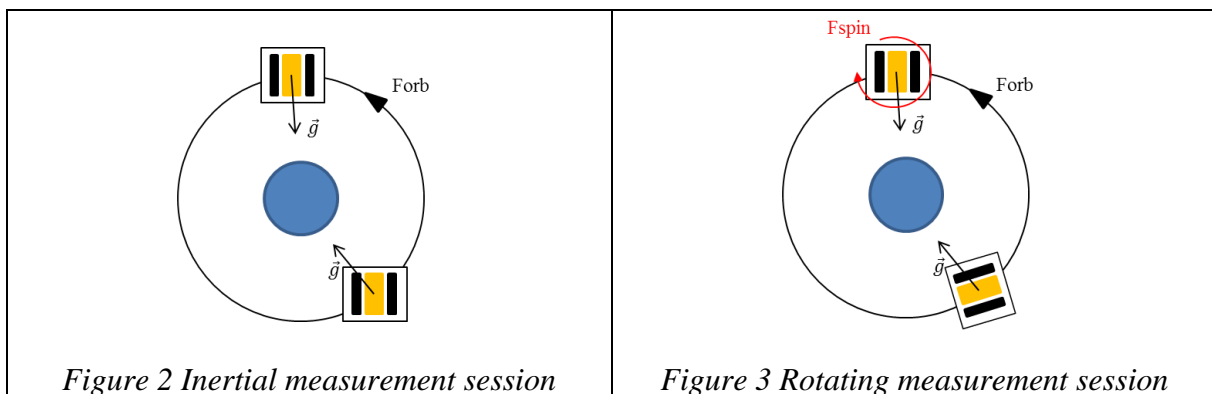
### *Rotating Sessions*

The satellite is set in rotation around the orbit's orthogonal axis ( $Y_{inst} \sim X_{sat}$ ) at the frequency  $F_{spin}$ : the EP signal is thus modulated at the frequency  $F_{ep} = F_{orb} + F_{spin}$ . These sessions last about 8 days (120 orbits): the session's length is a high level system parameter which determines the reduction of stochastic terms (by a  $\sqrt{T}$  ratio) while harmonic ones remain incompressible. Different spin velocities were used to improve the performance. Initially a first frequency was set at  $F_{spin1} = 7/2 \times F_{orb}$  and a second at  $F_{spin2} = 9/2 \times F_{orb}$ . But after in-flight testing, due to the high stochastic noise acting at low frequencies, it appeared that higher frequencies gave better performances. Thus a compromise was found with DFACS constraints to increase  $F_{spin1}$ : the upper limit was imposed by the gas consumption necessary to compensate inertial effects (centrifugal force and gyroscopic torque). In the end,  $F_{spin1}$  was moved up to the "SpinMax" rate of  $35/2 \times F_{orb}$  (5 times higher than the initial value).

### *Calibration Sessions*

In addition, specific sessions were dedicated to the accelerometer calibration. Based on an inertial pointing, they consist in performing different types of oscillations:

- angular sinusoidal oscillations of the satellite around its Y or Z axis of 0.05 rad (2.9 deg) at  $F_{cal} \sim 1.3$  mHz.
- linear sinusoidal acceleration of the TM at  $F_{cal} \sim 1.3$  mHz



## **Mission Scenario Management**

The mission scenario, which was weekly updated, is composed of a chaining of sequences, which can be mission sessions (inertial, rotating or calibration), technological sessions (for experiments), or technical sequences (for operational needs, such as guidance transitions). The scenario was managed by the Drag-Free Expertise Center (CECT). The CECT stands between the ground control center, the technological mission center (in charge of the expertise of a newly developed GNSS receiver), and the scientific mission center. The CECT had to take into account scientific needs and operational constraints to build a consistent scenario.

Seq #	Start (UTC)	Type of session	Perturbation	# of orbits	GN2 ZP (gr)	GN2 ZM (gr)
...						
248	2017-04-09T00:19:14.342850	TSNA	LUNE	55.40000	4.1	5.9
249	2017-04-12T19:49:21.801265		NO_ECLIPSE_NO_LUNE	1.01295	1.1	1.8
250	2017-04-12T21:29:44.784033	CAL_K1dxDFIS2_01_SUEP	NO_ECLIPSE_NO_LUNE	5.07000	4.7	8.1
251	2017-04-13T05:52:10.912485		NO_ECLIPSE_NO_LUNE	3.07939	11.1	10.6
252	2017-04-13T10:57:20.909821	EPR_V3DFIS2_01_SUEP	NO_ECLIPSE_NO_LUNE	106.00000	351.7	345.7
253	2017-04-20T18:01:55.033281		NO_ECLIPSE_NO_LUNE	1.51531	4.9	4.7
254	2017-04-20T20:32:05.041322	EPR_V3DFIS2_01_SUEP	NO_ECLIPSE_NO_LUNE	120.00000	394.4	392.5
255	2017-04-29T02:44:02.874511		NO_ECLIPSE_NO_LUNE	1.51531	5	4.2
256	2017-04-29T05:14:12.880945	EPR_V3DFIS2_01_SUEP	NO_ECLIPSE_NO_LUNE	120.00000	392.9	392.6
257	2017-05-07T11:26:10.798985		NO_ECLIPSE_NO_LUNE	2.57703	3.6	5.3
258	2017-05-07T15:41:33.772832	CAL_tetadYDFIS2_01_SUEP	NO_ECLIPSE_NO_LUNE	5.07000	3.3	7.5
259	2017-05-08T00:03:59.903077		NO_ECLIPSE_NO_LUNE	1.18063	2.8	3.9
260	2017-05-08T02:00:59.907739	CAL_deltaYDFIS2_01_SUEP	NO_ECLIPSE_NO_LUNE	5.07000	11.8	15.7
261	2017-05-08T10:23:26.037984		NO_ECLIPSE_NO_LUNE	1.18282	1	1.7
262	2017-05-08T12:20:39.064346	CAL_tetadZDFIS2_01_SUEP	NO_ECLIPSE_NO_LUNE	5.07000	3.7	7.7
263	2017-05-08T20:43:05.192798		NO_ECLIPSE_NO_LUNE	1.01295	0.6	1.4
264	2017-05-08T22:23:28.175207	CAL_K1dxDFIS2_01_SUEP	NO_ECLIPSE_NO_LUNE	5.07000	3.9	7.5
265	2017-05-09T06:45:54.301867		ECLIPSE	0.00000	0	0

Figure 4 Excerpt of the mission scenario

Figure 4 shows an excerpt of the mission scenario. This excerpt is representative of the chaining of scientific sessions performed between two Moon-dazzling periods:

- Once a month, the star-tracker (STR) is dazzled by the full Moon. DFACS has then to be switched to coarse mode with drag free OFF (non-propulsive mode using MTQs), which leads to an interruption in the scientific mission. Technical sessions (like #248) are thus scheduled each month to manage this periodic event.
- In this excerpt, the drag-free is performed with the SU-EP test mass (Pt,Ti TM: see Figure 1).
- The whole sequence is dedicated to measurements in ‘Spin Max’ rotation mode with three scientific sessions of a hundred orbits each (#252, #254, #256).
- In addition, shorter calibration sessions (5 orbits each) are scheduled before and after each chaining of scientific sessions.
- The last two columns show the estimated gas consumption per wall for each session (in gram). Most of the gas is spent by the ‘Spin Max’ sessions because of their duration.
- At the end of this excerpt, Microscope enters the annual eclipses period. The thermal stability of TSAGE is perturbed, and the measurements have to be stopped.

## Microscope Satellite

### Platform

The Microscope spacecraft (see Figure 7) is based on the Myriade satellite productline. These satellites, developed by CNES, EADS Astrium (now AirbusDefense & Space) and Thalès AleniaSpace, are 200 kg class satellite with a common (but customizable) platform and an adaptable payload. The rationale underlying their manufacturing is to offer to the scientific community low-cost platforms. This has been achieved thanks to miniaturized electronics, the use of components off-the-shelf and an aimed reliability lower than for other satellites but still leading to an acceptable lifetime, thus inducing downsized costs via the deletion of redundancies, etc.

Other CNES scientific satellites of the family are Demeter (seismology, 2004), Parasol (aerosol observation, 2004), Picard (sun observation, 2010), Taranis (energetic magnetic phenomena, tentative launch date 2020) and MicroCarb (atmospheric carbon dioxide measurements, tentative launch date 2021). The new generation platform, Myriade Evolution is on its way with the Merlin spacecraft (tentative launch date 2024).

The Microscope mass is close to 300 kg due to specific characteristics of the payload and the mission requirements. In particular, standard Myriade satellites use Hydrazine-based propulsion system while Microscope needed a specific one. Besides, Microscope also included a deorbit system – in order to be compliant with the French space operations act – that adds mass.

The TSAGE payload, located at the center of the satellite, was entirely manufactured and tested by the ONERA laboratory. As prime contractor, CNES designed and integrated the platform and also operated the spacecraft in-orbit.

### **Drag-free Attitude Control System (DFACS)**

Eq. 1 is true with perfect sensors. Actually, measurements contain some parasitic terms that have to be considered. More precisely, 40 sources of error have been exhaustively studied in the error budget and the most significant among them comes from differential scale factors, and from the miscentring between the two masses. Scale factors are known at 0,01% and maximal offcentring is 20 $\mu$ m.

Basically, the error budget is shared equally between all sources of error, which means that each error terms (including drag-free and attitude control performance) must be inferior to an allocation of  $7,5 \cdot 10^{-15} \text{m.s}^2 / 40 \approx 2 \cdot 10^{-16} \text{m.s}^2$ .

Finally, to achieve the performance required for the mission, the DFACS most stringent requirements in mission mode are (see [1]):

- Residual linear accelerations lower than  $10^{-12} \text{m/s}^2$
- Angular acceleration lower than  $10^{-11} \text{rad/s}^2$
- Angular rate stability better than  $10^{-9} \text{rad/s}$

To achieve this ambitious performance, the satellite has to protect the payload from all non-gravitational forces disturbing measurements. Actually Microscope does not implement a traditional “drag-free” (where the test mass would freely float), but it could be defined as an “accelerometer-mode” drag-free satellite: the TM is suspended and the satellite provides an additional layer of control. That’s why the acronym AACS (Attitude & Accelerations Control System) is generally preferred to DFACS (Drag Free Attitude Control System). This observation is of first interest to understand our management of TSAGE linear biases. Indeed, we were allowed to subtract the ‘estimated linear biases’ from the measurement of the DF-TM, which is of great interest regarding the gas consumption management.

Once the DFACS is active, a frequency based separation operates. The s/c propulsion system compensates for external perturbations (6 DoF) at low frequency (up to some tens of mHz, including Fep). In the meanwhile, the suspension of the TM (6 DoF) is loaded by biases and higher frequencies (transient and spikes).

Since the EP violation signal should be a sine at Fep frequency, the DFACS most stringent requirements are at Fep. On linear axes, the residual linear accelerations in mission mode must be less than  $10^{-12} \text{m/s}^2$  in the bandwidth of scientific interest. The angular control is also submitted to stringent requirements to limit angular toward linear coupling, due to the TM miscentring.

To meet these stringent requirements, the DFACS relies on the payload accurate accelerations measurements for both linear and angular control. Linear accelerations measurements are directly used by the drag free control whereas the attitude estimation is the result of hybridization between STR measurements and angular accelerations measurements. Then a set of 8 cold gas thrusters allows to accurately realize the commanded thrust.

The DFACS control loop is illustrated in Figure 5.

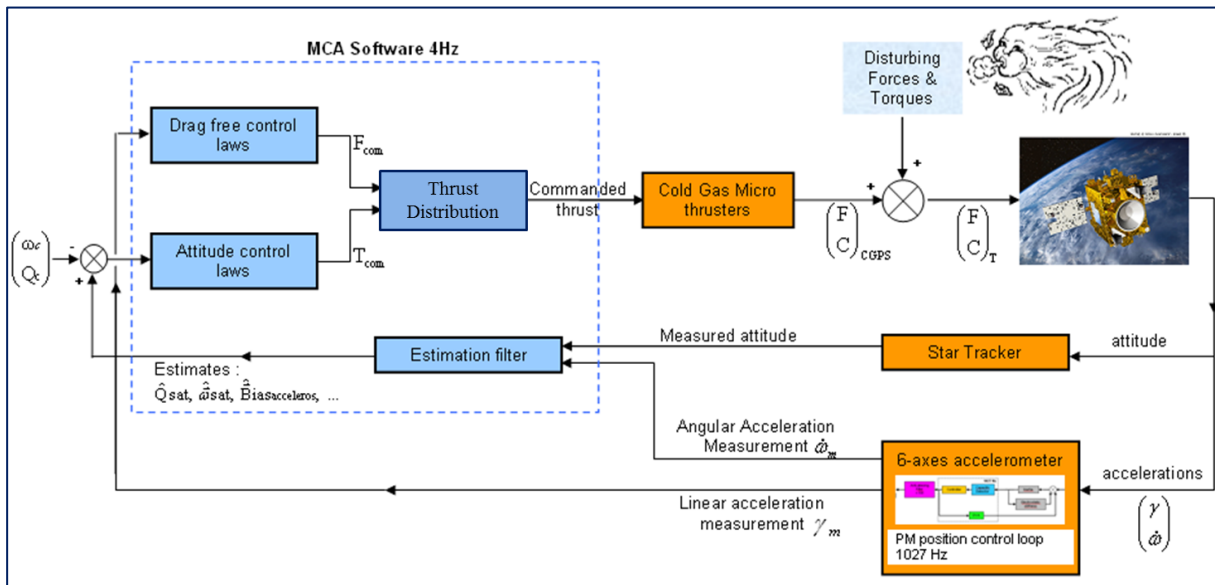


Figure 5 DFACS control loop

## The Cold Gas Propulsion System

### Overall Presentation

The spacecraft architecture was designed in such a way that two opposite and identical panels were used for propulsion system (see Fig 7).

The concept of CGPS ([2]) is based on a piezo-actuator regulating the propellant flow (Nitrogen) of a micro-nozzle, ensuring a continuous thrust regulation between  $1\mu\text{N}$  and  $500\mu\text{N}$ . More precisely, the CGPS is composed of two identical subsystems called CGPSS (one on +Z panel and the other on -Z panel). Each CGPSS includes 4 modules:

- The GDM (Gas Distribution Module) is composed by the tanks and its only purpose is to stock the high pressure gas. The tanks are made of composite material with a metallic liner. GDM stores and maintains the gas at its operational range (pressure and temperatures). A GDM is filled with 8.25 kg of gaseous Nitrogen stored at the maximum pressure of 345 bars.
- The PRM (Pressure Regulation Module) provides the gas distribution to the thrusters, and contains all the equipment units necessary to ensure the pressure regulation of the CGPS. It is composed of a high pressure part and a low pressure part. The high pressure part includes mainly valves, pressure transducers and a pressure regulator. The low pressure part is composed of valves, pressure transducer and a plenum ( $\sim 0.7$  L capacity). The main function of the PRM is to deliver a 1 bar pressure to the thrusters throughout the mission lifetime. In order to prevent slam-start on the low pressure stage at HPLV opening with pressure regulator opened, a sonic orifice has been mounted between the HPLV and the pressure regulator.
- The TRM (Thrust Regulation Module) is composed of the 8 thrusters (4 nominals and 4 redundants). The micro-thrusters (MTs) operate in a close-loop configuration using a miniaturized Mass Flow Sensor (MFS) as thrust measurement probe and piezo-electric actuator to modify the nozzle section and modulate the gas flow. The qualification of such micro-thrusters has been achieved in 2011 in the frame of GAIA, so it was not available at the beginning of 2000s.
- The ECM (Electronics Control Module) contains the electronics items necessary to provide the power supply to all the CGPSS modules. It controls the TRM thrust, and ensures the avionic interface with the On Board Computer. The ECM is the link between the on-board computer and the whole CGPS active equipment (valves, pressure

transducers, thrusters, etc.). It collects TM from the CGPS and sends it to the OBC as well as receives orders from the OBC. The thruster's control loops are included in the ECM.

During the mission, only the 8 nominal thrusters (4 for each CGPSS) were actuated at the same time.

The CGPSS schematic is presented on Figure 6.

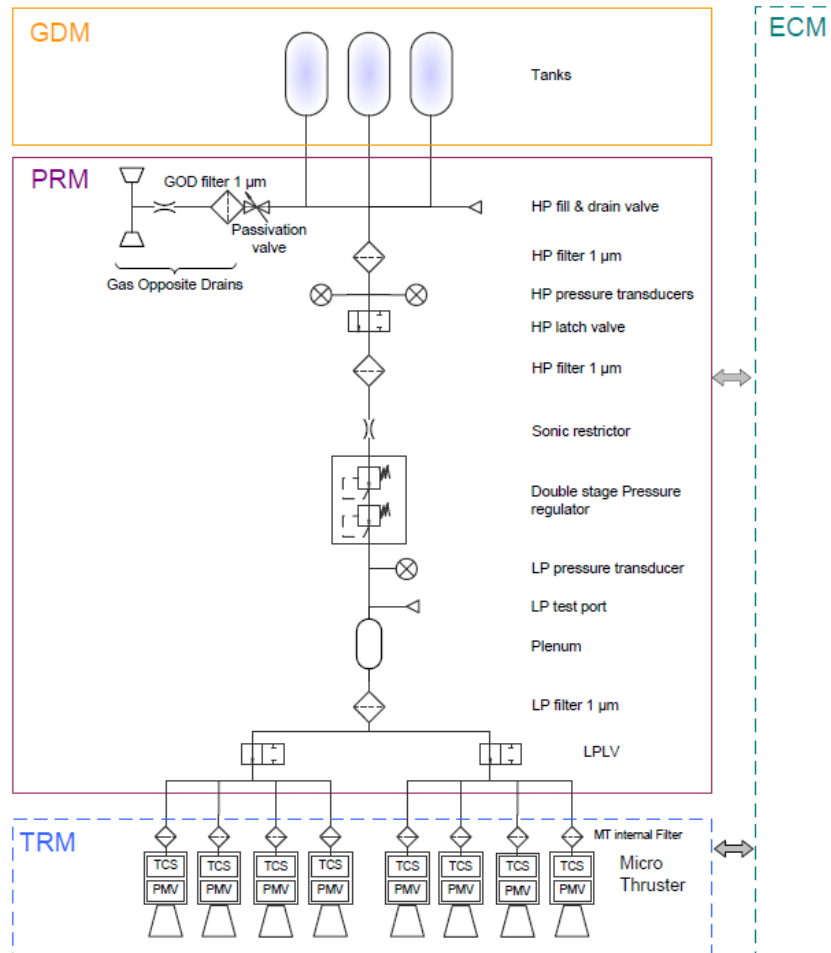


Figure 6 CGPSS schematics

### Micro-Thrusters

The Micro-Thrusters are manufactured by the Leonardo company (Milan and Florence, Italy) and are off-the shelf equipment. They have been qualified within the frame of the ESA GAIA program. The basic principle is that gas at constant pressure is fed to the thruster. This gas expands through a nozzle thus creating a thrust. This thrust ought to be adjustable and that action is performed using a needle that will let the needed quantity of gas flow (hence managing the thrust).

An MT is composed of two main pieces of equipment which are the Thruster Valve (TV, actuated through piezoelectric disks) and the Mass Flow Sensor (MFS). The TV is the actuator that allows regulating the mass flow rate. The MFS is the sensor that reads the mass flow rate and sends this data to a 50Hz closed loop implemented inside the ECM. Thrust ranges for Microscope mission vary from 1  $\mu\text{N}$  to 300  $\mu\text{N}$  (specification from DFACS, late enhanced to 500 $\mu\text{N}$  according to GAIA requirement/performances to shorten the attitude changes) with a

resolution of  $0.2 \mu\text{N}$ . The TV's nozzle is millimeters long and its throat diameter around several hundreds of microns.

The ECM control loop's principle is that the thrust command is sent to a PID controller that will determine the voltage to apply to the TV's piezo-electric disks. The voltage is updated every 20 ms according to Mass Flow Sensor output. The thrust set point is updated from DFACS every 250 ms. The thrust's time response is specified as 250 ms at 63 % of thrust step.

The MFS needs to be calibrated. Indeed, MFS' output is a voltage that represents the mass flow rate. The valve has to be closed periodically and the associated voltage recorded inside the ECM in order to have a reference voltage. This voltage is the "zero mass flow rate" reference voltage also called "offset". During thruster operation, the ECM subtracts this offset to the mass flow rate voltage output in order to determine the mass flow rate physical value. Each thruster has its own offset value. The idle must be compatible with the drift of this offset in order to avoid divergence of the local control loop. The idle was set to  $2.5 \mu\text{N}$  for Microscope (zeroing procedure activated once a month). Idle was stable in scientific operation even at the end of the month. A thruster at idle is perturbed by strong and sudden variations on the branch (fluidic interactions). However, these phenomena were limited to transient phases (out of science time).

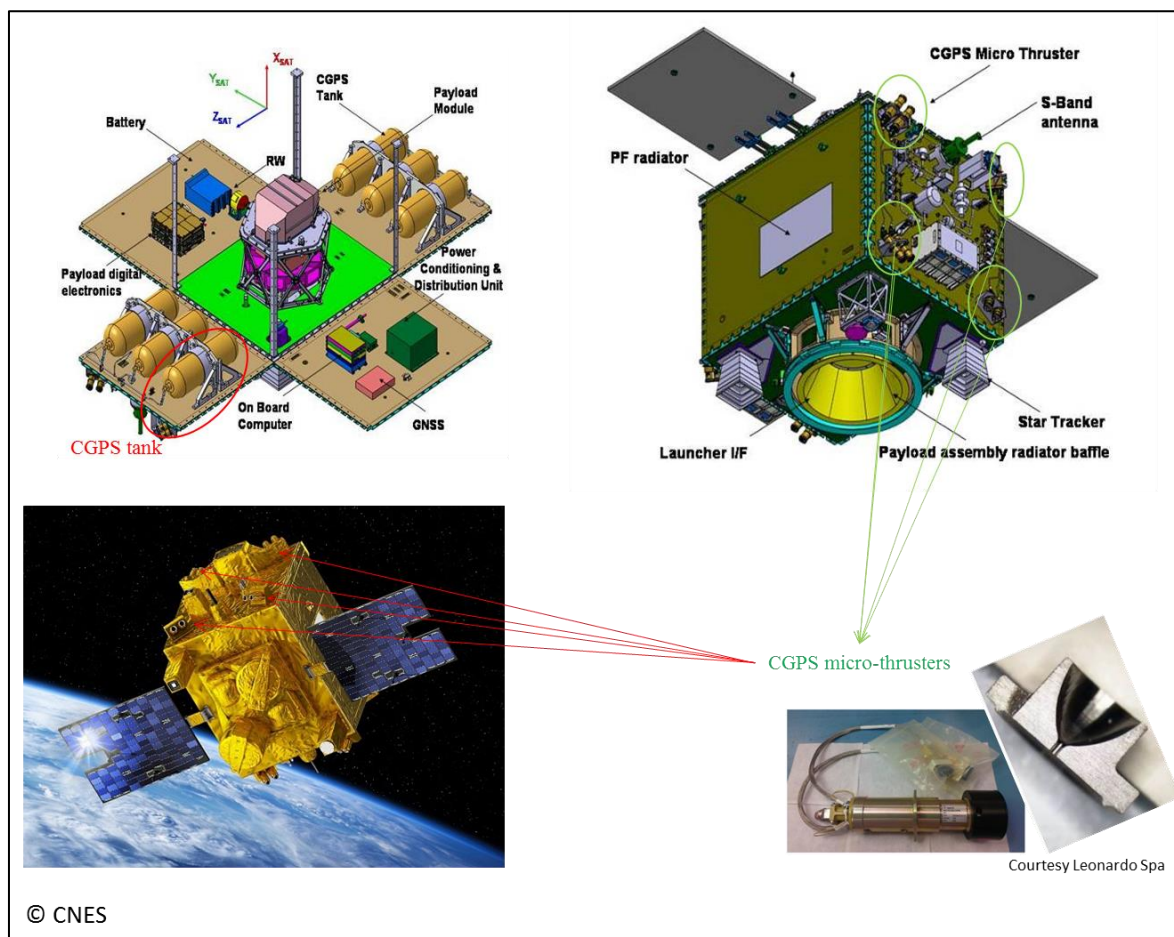


Figure 7 Microscope Cold Gas Propulsion System

## Dimensioning Process of the CGPS Architecture

### Propulsion Type

Other Myriade satellites don't need any drag-free capacity, so they don't have actuators adapted to linear control. For this kind of control, a propulsion system is needed. The Myriade product line uses a Hydrazine propulsion system in the 1N range, this system is dedicated to impulsional

orbit control one million time less accurate than what the Microscope's mission needed. This Hydrazine propulsion was therefore not relevant in the frame of the Microscope's mission.

Hybrid solutions for DFACS, i.e. systems using different actuators for angular and linear control were rejected. Indeed, the use of reaction wheels would have caused micro dynamical disturbances on the payload (which was observed later during a dedicated end of life experiment) and magnetotorquers (MTQ) would have generated magnetic perturbations. Therefore, it was necessary to choose a propulsion system able to achieve simultaneously drag-free and attitude control.

Early in the development, the Field Emission Electric Propulsion (FEEP) technology was intended to be used in the propulsion system ([3]). The main asset of this technology is the very high expected Isp (several thousands of seconds) hence the very low propellant mass needed to perform the mission. However, after a first preliminary design phase, the maturity of this technology has been deemed too low to pursue. That is why, the cold gas technology was chosen in 2009. The expected Isp is much lower (up to a hundred seconds depending on the gas) but at that time, the maturity of the technology was already high as the micro-thrusters to be used on Microscope were scheduled to fly on the GAIA spacecraft and were being qualified. Therefore, this technology was considered the best compromise between performances and TRL level.

### Architectural Choices

The propulsion configuration (position and orientation of the thrusters) was mainly driven by attitude control considerations:

- First, it can be demonstrated that at least 8 nozzles are necessary to perform a 6-axis control with monolateral thrusters.
- Then, we quickly observed that torques were higher than forces and were quite symmetrical. That's why the thrusters were located on the corners (the farthest from the satellite center of mass) for a maximum torque efficiency.
- Finally, the thrusters' orientation (azimuth and elevation) was optimized through a comparison between the 6 DoF "control authority domain" and the 6 DoF "perturbations domain" (see [4]).

Moreover, an important design driver was the integration and test effectiveness:

- First, in order to perform propulsion integration in parallel to the overall satellite AIT sequence (mainly to work separately from the payload located in the center of the satellite), we chose to implement the propulsion system on independent and autonomous propulsive walls (+Z and -Z) called CGPSS (see Figure 6);
- The two walls were also designed to be independent from each other (as seen in Figure 7). Indeed, any fluidic link between them would have made the integration much more complex (and not compatible with Myriade AIT principle and GSE). At the end, this choice had a non negligible impact on DFACS monitoring because it led us to manage carefully the differential gas consumption between the two walls all along the mission.

Finally, a 1(+1) redundancy on Microthruster only has been decided. The GAIA in-flight feedback was not available at the time. Furthermore, due to the small size and mass of the micro-thrusters this redundancy was not a dimensioning constraint on the mass and volume budget of the satellite.

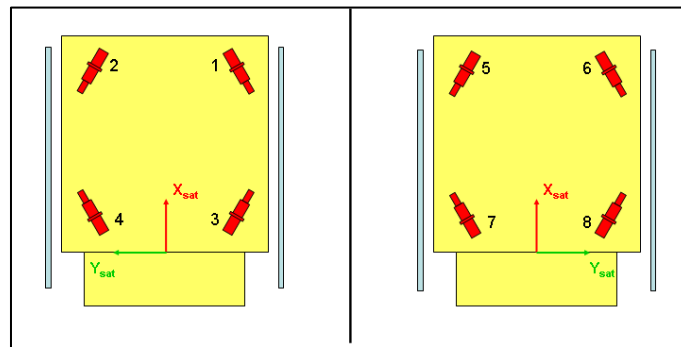


Figure 8 CGPS nominal configuration

## Gas Consumption Studies

During the design phase of the mission, gas consumptions studies were conducted in order to:

- check the feasibility of the mission.
- identify the main parameters impacting the gas consumption.
- build consumption predictions depending on the guidance, to be used at a system level to update the mission scenario.

Monte Carlo analyses were performed, using an adapted DFACS study simulator. Models were simplified to work at low frequency (0.02 Hz) in order to be able to simulate the entire mission within an acceptable CPU time.

Different mission scenarios were tested to determine if the amount of gas would be sufficient to complete the mission. These scenarios were designed to characterize different level of achievement of the scientific objective. They were composed of representative sequences of sessions in all 3 guidance modes (inertial, rotating and calibration) for different mission durations. The results of the Monte Carlo analyses showed that 100% of each tested scenario could be completed with the nominal amount of 8.25kg of nitrogen per wall.

To identify the major contributors to the gas consumption, many parameters were dispersed, such as:

- the characteristics of the propulsion system (Isp, idle, position and alignment uncertainties),
- the satellite characteristics (inertia, mass, centering),
- the external perturbations (altitude, solar activity, magnetic momentum),
- other possible contributors of the DFACS control loop (including TSAGE).

As expected, the analyses highlighted the impact of high solar activity for low altitudes (increased air-drag), thus drowning the effects of other parameters for these settings. Apart from that, the major identified contributors were:

- the Isp: Isp hypotheses were deduced from MT characterizations performed by ONERA and TAS-I (e.g.: uncertainty from 50s to 57s for a 30 $\mu$ N thrust). High Isp characteristics proved to significantly increase the life time of the mission.
- The satellite residual magnetic momentum (battery, magnetic shield of the scientific instrument, valves, etc) was the first contributor to gas budget in case of low solar activity (torques in the range 50 $\mu$ N.m),
- the satellite inertia: strong values of Ixx and Iyy inertia increased the gas consumption (Iyy-Izz causing gravity gradient torque).
- TSAGE linear bias: the compensation of the residual of the “estimated linear biases” by the AACS (see DFACS section) could lead to a significant increase in consumption. This conclusion led us to closely monitor the evolution of the biases all along the mission.

A useful outcome of this study was an estimation of the consumption for each type of scientific session (type of guidance, TM used for DFACS). Table 1 presents an extract of the results (in gram per orbit per wall). We can note that:

- The ‘SpinMax’ rate (35/2xForb) was not foreseen at the time of the study, thus no prediction was done concerning this guidance mode.
- There are very few distance between each guidance type (inertial effects are small). With the mission design solar activity hypotheses, the main contributor to the consumption is the air-drag which overcomes the other effects.
- The gap between the two walls is linked to the TSAGE residual linear biases hypotheses.

Table 1 Example of prediction of the gas consumption (in gram per orbit per wall)

Session type	Z+	Z-
<b>Inertial</b>	1.1	1.7
<b>Low spin (7/2xForb)</b>	1.3	1.5
<b>Medium spin (9/2 x Forb)</b>	1.3	1.5
<b>Calibration (angular oscillation)</b>	1.2	1.6

### In-Flight Performance: Gas Consumption Monitoring

The short term monitoring of the cold gas consumption was performed within the Drag-free Expertise Center (CECT), [5].

The algorithm uses the real gas law, which links the pressure, temperature and volume of a gas, in our case the Nitrogen ( $N_2$ ) contained in the tanks.

For each wall +/-Z, the measurements of high pressure sensors are combined to deduce the pressure inside the tanks. The temperature of each tank #i (i from 1 to 3 as shown in Figure 7) is measured through temperature sensors. We can then deduce the volumic mass  $\rho_i$  in a given tank by interpolating the nitrogen’s NIST (National Institute of Standard and Technology) lookup-table. Then the gas mass for a given wall (+/-Z) is computed by applying the volumic mass to the volume of the corresponding tanks:

$$Mass_Z = \sum_{tanks} \left( \rho_{NIST_{N_2}}(P_Z, T_{tank_i}) \times Vol_{tank_i} \right) \quad Eq. 3$$

where

- $Mass_Z$  is the consumed mass of gas for a given wall (+/- Z)
- $P_Z$  is the measured pressure for the given wall
- $T_{tank_i}$  is the measured temperature for a given tank
- $\rho_{NIST_{N_2}}$  is the volumic mass of nitrogen corresponding to these pressure and temperature
- $Vol_{tank_i}$  is the volume of the considered tank

It was then possible to infer the consumption of each sequence in the scenario by computing the decrease of the gas mass of each wall.

The sequences were categorized in several types depending on criteria such as the guidance, the TM used on-board in the DFACS, the satellite mode ... A statistic was then drawn to evaluate the dispersion of the consumption of each type. Using these statistics, it was possible to foresee the gas consumption of the future sequences in the mission scenario. The future evolution of the gas mass was regularly computed (for each update of the scenario, using the latest gas consumption statistic) and the prediction was taken into account carefully in the scenario update processed by the CECT.

Figure 9 shows the gas consumption per orbit as a function of the sequence type for all the scientific sessions performed during the mission, and Figure 10 shows the evolution of the mass decay all along the mission.

By comparing these in-flight results with the predictions, we can note that:

- The variability for a given type comes from the evolution of the accelerometer biases (inducing a residual with respect to the estimated values taken into account in the AACS on-board). This is consistent with the studies which showed a high impact of the biases on the consumption.
- The major gas consumer sessions are the SpinMax sessions, with  $\sim 3.3$  g/orb/wall. These were not considered in the prediction study, but according to the results for the lower spin sessions a higher consumption was not foreseen at first. Actually, the high spin rate creates a high gyroscopic torque due to the non-diagonal inertia of the satellite ( $I_{xz}$ ), whose control increases the consumption.
- The second most consuming sessions are calibration ones. The higher level observed in-flight compared to the prediction is due to a change in the oscillation characteristics. Indeed, the consumption is due to the torque necessary to create the angular oscillation of the satellite.
- For the other type of guidance (inertial or slow rotating), the optimal consumption (with small TSAGE biases residuals) is  $\sim 0.6$ g/orbit/wall. This is half the predicted value. Actually, the solar activity was very low during the mission so that air drag remained negligible ( $<2.5\mu\text{N}$ ).

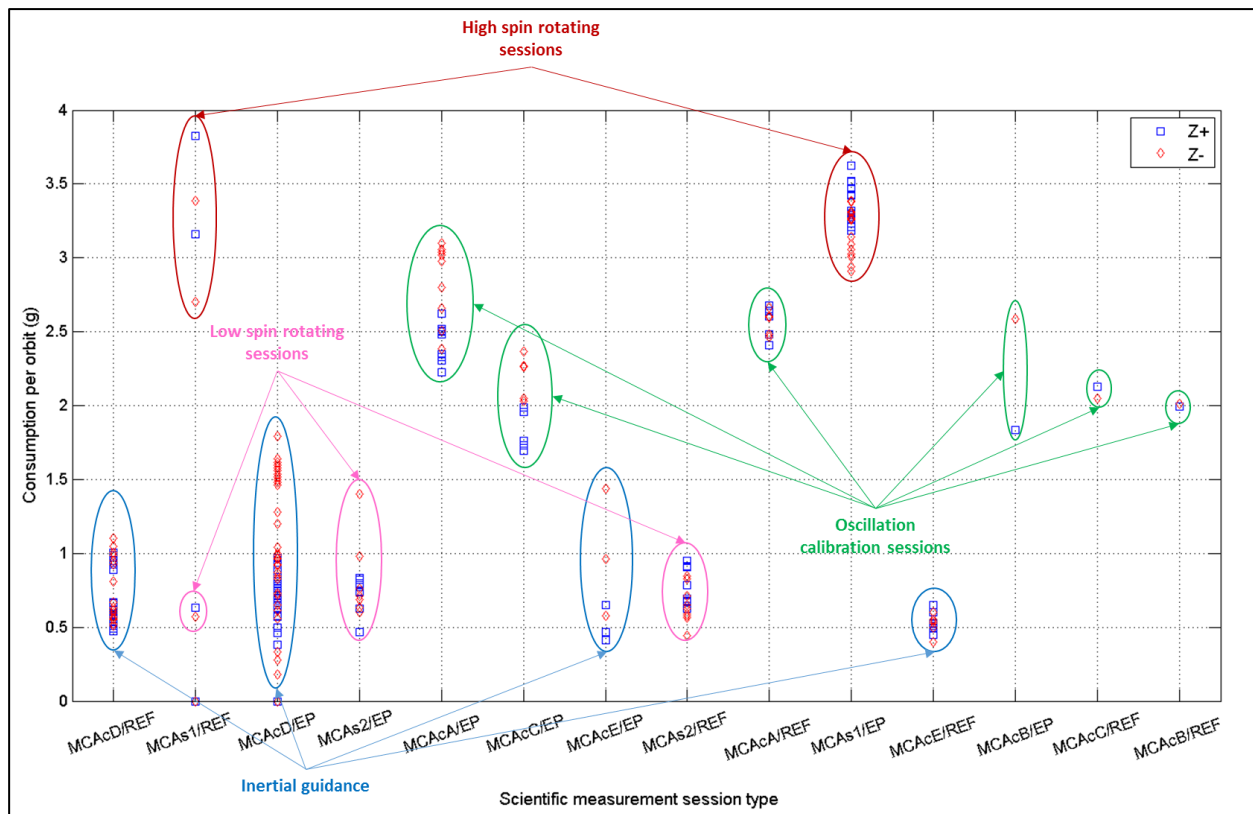


Figure 9 Gas consumption statistics w.r.t. the guidance type (g per orbit per wall)

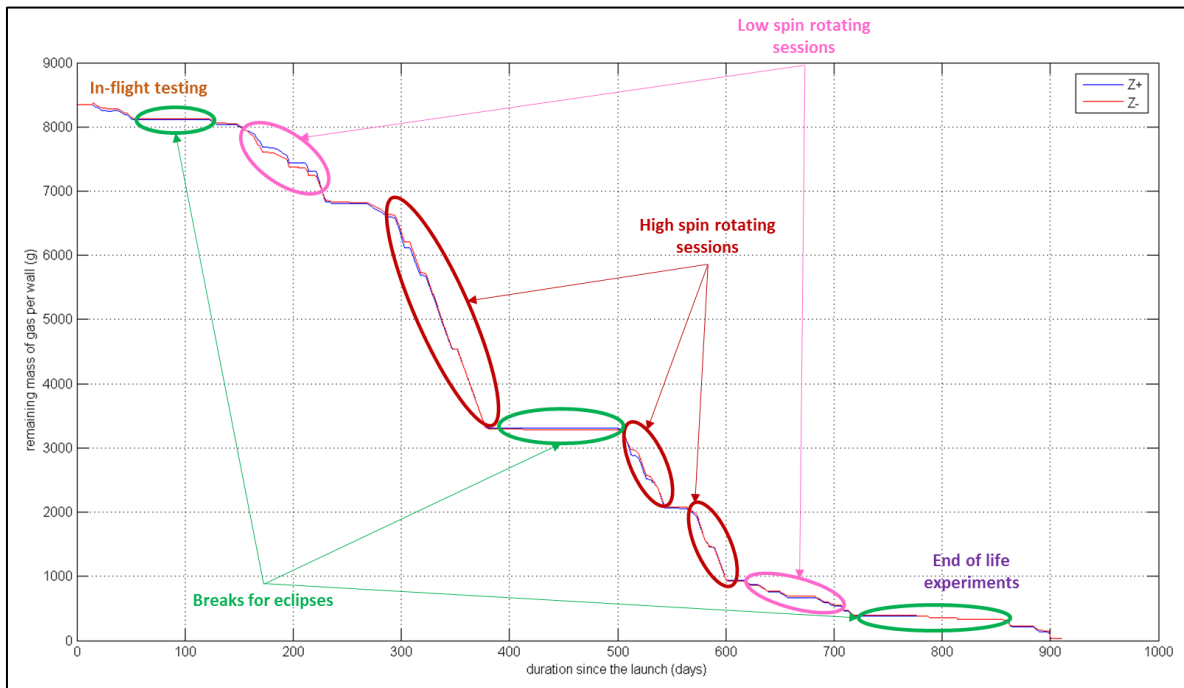


Figure 10 Evolution of the gas mass along the mission (g per wall)

## End-of-Life Experiments

### Thrust Calibration

#### Gas Consumption Monitoring

The PVT method used for monitoring was the nominal one. An alternative method, named Pulses Counting, was also implemented using sensor-independent telemetry data: by integrating the thrusts  $T_j$  commanded to each thruster # $j$  ( $j$  from 1 to 4 for each wall +/-Z) by the DFACS, we can deduce the theoretical gas consumption (GC) over a time period:

$$GC_Z = \frac{\sum_{j=1..4} \left( \int_{t_0}^{t_1} T_j \cdot \Delta t \right)}{g_0 I_{sp}} \quad Eq. 4$$

Where  $g_0$  is the standard acceleration due to Earth gravity and  $I_{sp}$  is the average specific impulse.

This alternative method was used as replacement for the nominal method in the case of very short sessions (the measurement noise leads to inaccurate PVT results for sessions shorter than 2 orbits) or thermal transitions (in case of high temperature's gradients, the delay in the temperature's sensors tends to distort the PVT results). We also used it to calibrate the mass flow across the thrusters (comparison between the 'commanded' flow and the measured one).

By comparing the monitoring results of the two methods (PVT and Pulses Counting), a discrepancy of 25% was observed on the mass flow for all the sessions longer than 5 orbits (i.e. with a good signal over noise ratio for the PVT method). This led us to suspect a possible under-calibration of the propulsive system.

### “Tangential Thrusts” Experiment

In addition to these observations, an end-of life experiment was performed in order to calibrate the propulsive sub-system using orbit determination and TSAGE measurements. In this experiment, the satellite pointing is geocentric and three levels of tangential thrusts ( $50\mu\text{N}$ ,  $250\mu\text{N}$  and  $500\mu\text{N}$ , orbital frame) were applied during one orbit each (drag-free OFF). In order to balance the orbital effect such as air-drag, thrusts in the opposite direction were also applied later. After each thrust, three more orbits were used for orbit restitution. Two geocentric pointing were tested (+Zsat and -Ysat at nadir) in order to change the projection from the local orbital to thruster axes. For the Zsat at nadir configuration 2 MT from each wall were mainly loaded, whereas for the -Ysat at nadir configuration the 4 MT on one wall were active (see Figure 11).

The thrusts can be observed through TSAGE linear acceleration measurements. A comparison between the measured thrusts (TSAGE acceleration  $\times$  mass) and the commanded ones shows a mean under-efficiency of -20%.

This value is confirmed by an estimation of the thrusts performed through the orbit determination process following two methods:

- A direct method with an adjusted constant along track acceleration during thrust period, i.e. one orbit. The other adjusted dynamic parameters are solved thanks to two periods of three orbits defined just before and after the thrust.
- A comparison of a theoretical and an estimated evolution of the semi-axis.

The orbit determination process uses GPS measurements obtained with a new spatial single-frequency GPS receiver manufactured by SYRLINKS and named G-SPHERE-S. These measurements are pre-processed thank to an ionosphere-free combination.

An under-consumption is also observed in the same ratio so that the Isp hypothesis is respected. The -20% discrepancy probably comes from the calibration ‘thrust to MFS voltage’ performed on ground.

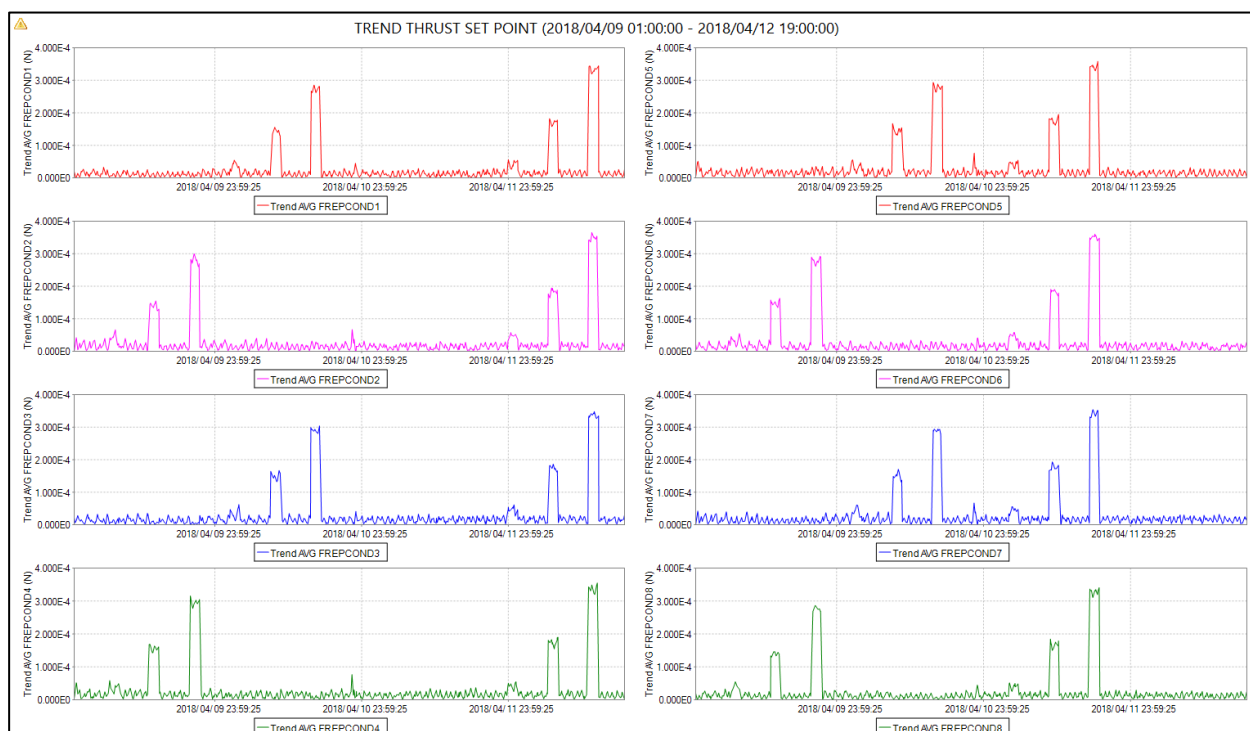


Figure 11 “Tangential thrusts” experiment: commanded thrusts (N, left =  $Z_p$ , right =  $Z_m$ )

## “Increased Idle” Experiment

The purpose of this experiment is to test the overall propulsive sub-system for high thrust levels (i.e. several hundred  $\mu\text{N}$ ). The corresponding performance (noise, response time) is indeed of great interest for future missions (like Euclid).

The experiment consists in increasing the micro-thrusters’ idle progressively from  $2.5\mu\text{N}$  up to  $200\mu\text{N}$  and then decreasing it straight down to  $2.5\mu\text{N}$ . Each value of idle is kept for one orbit before switching to the next value. The selected guidance is geocentric in order to insure that the main perturbations are periodic at the orbital frequency. Figure 12 shows the MTs’ commanded thrust along the experiment. The different set points are clearly visible on all 8 MTs. It can be noted that the thrust level translation is greater than the idle’s increment, especially for idles  $\geq 100\mu\text{N}$ . This behavior is consistent with the thrust distribution algorithm for high thrusts.

The commanded forces and torques are computed by DFACS in closed loop (drag-free ON) to counter the perturbations (mainly periodic in geocentric mode). In Figure 13 and Figure 14 a sudden change can be observed for high idle levels ( $100\mu\text{N}$  and  $200\mu\text{N}$ ). This loss of periodicity is a direct effect of the idle increase. For a  $200\mu\text{N}$  idle the commanded tensor variation is  $[20\mu\text{N} ; 20\mu\text{Nm}]$ , which represents 5% of the maximal commanded thrust for this set point. This performance is consistent with the 5% scale factor specified for each MT. Moreover, the DFACS overall performance is independent from idle, showing that the propulsion system keeps its performance (response time, noise, linearity, etc.) even heavily loaded.

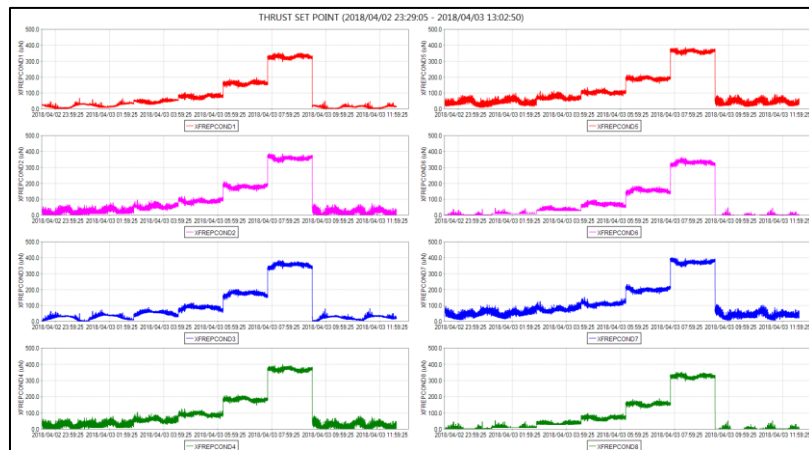


Figure 12 Increased idle experiment : commanded thrusts

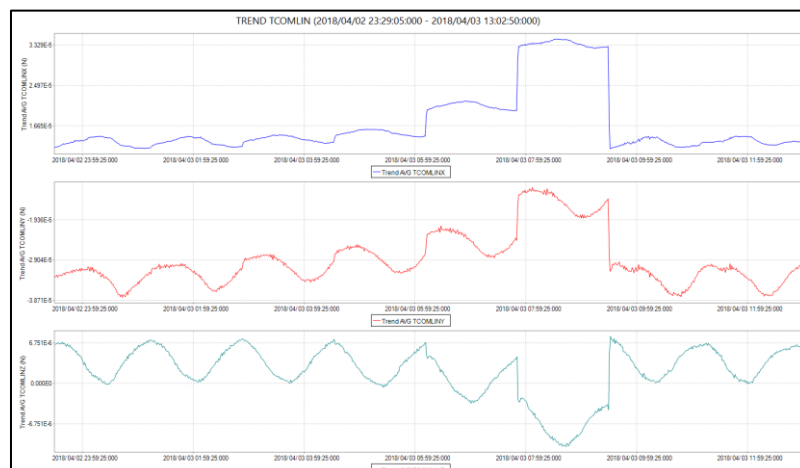


Figure 13 Increased idle experiment : commanded Force (SL frame)

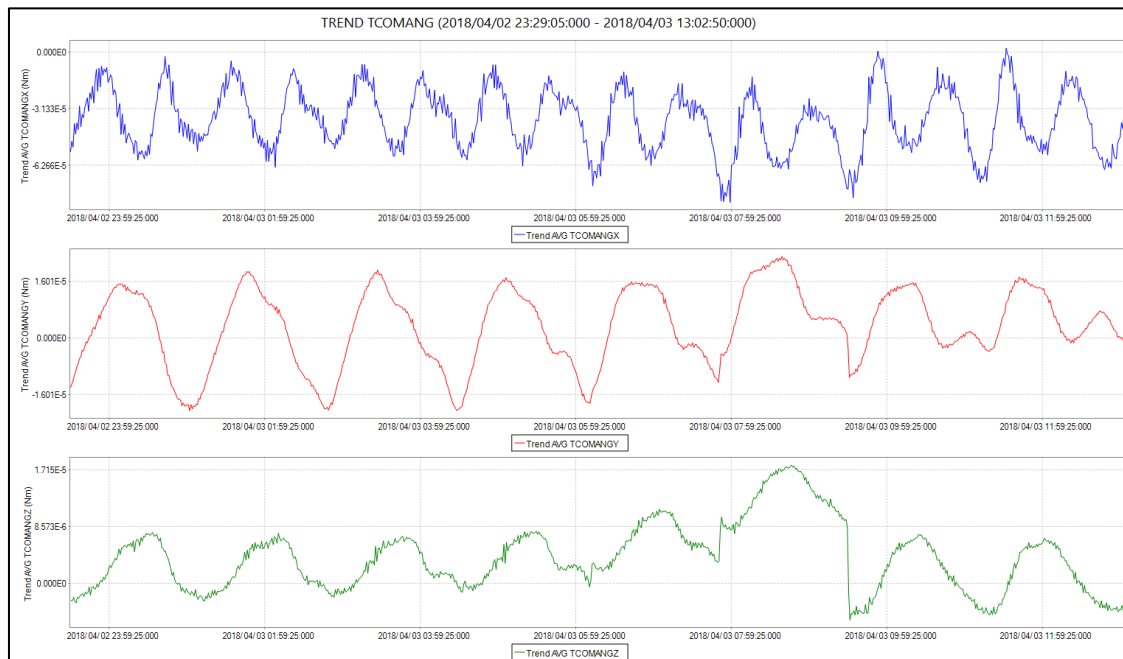


Figure 14 Increased idle experiment : commanded Torque (SL frame)

### “Redundant Propulsive Configuration” Experiment

Along the whole scientific mission, only the nominal thrust configuration was activated. In order to get more feedback about the performance and reliability of the propulsive system, the redundant configuration was activated over 48 hours: after in flight testing and calibrations, 22 orbits of drag-free in inertial mode were realized.

The analysis of DFACS performance showed no impact on the control system behavior. This experiment took place during the eclipses season. Despite that, the drag free performance is lower than  $1.10^{-13} \text{ m/s}^2$  @Fep, that is 10 times better than the expected value (3 axes)! The performance of the 8 redundant thruster is then fully confirmed.

Moreover, the comparison of the monitoring results of the PVT and Pulses Counting showed a -10% under-consumption (to be compared to the -25% for the nominal configuration). The under-calibration of the redundant batch seems slightly different than the nominal one.

### Thrust calibration via TSAGE

A specific AACS mode named MCAcp stabilizes the s/c in inertial attitude and then inhibits the control and activates the thrusters (DFACS in open loop) one by one for 10 seconds for different set-points from  $5\mu\text{N}$  up to  $300\mu\text{N}$ . The objective was to demonstrate the efficiency of the CGPS and the sensitivity of TSAGE. This can be seen on Figure 9 (example of the  $5\mu\text{N}$  set-point). The commands are plotted on the top figure, each one of the 8 thrusters is successively commanded to  $5\mu\text{N}$  while the others remain to idle ( $2.5\mu\text{N}$ ). The accelerations of the s/c measured by the 4 TMs are displayed below (example of Y axis). One can see the rise and fall time. Such an acceleration step ( $2.5\mu\text{N}/301.4\text{Kg}=8.3\text{e-}9\text{m/s}^2$ ) is easily measured here with a good signal to noise ratio.

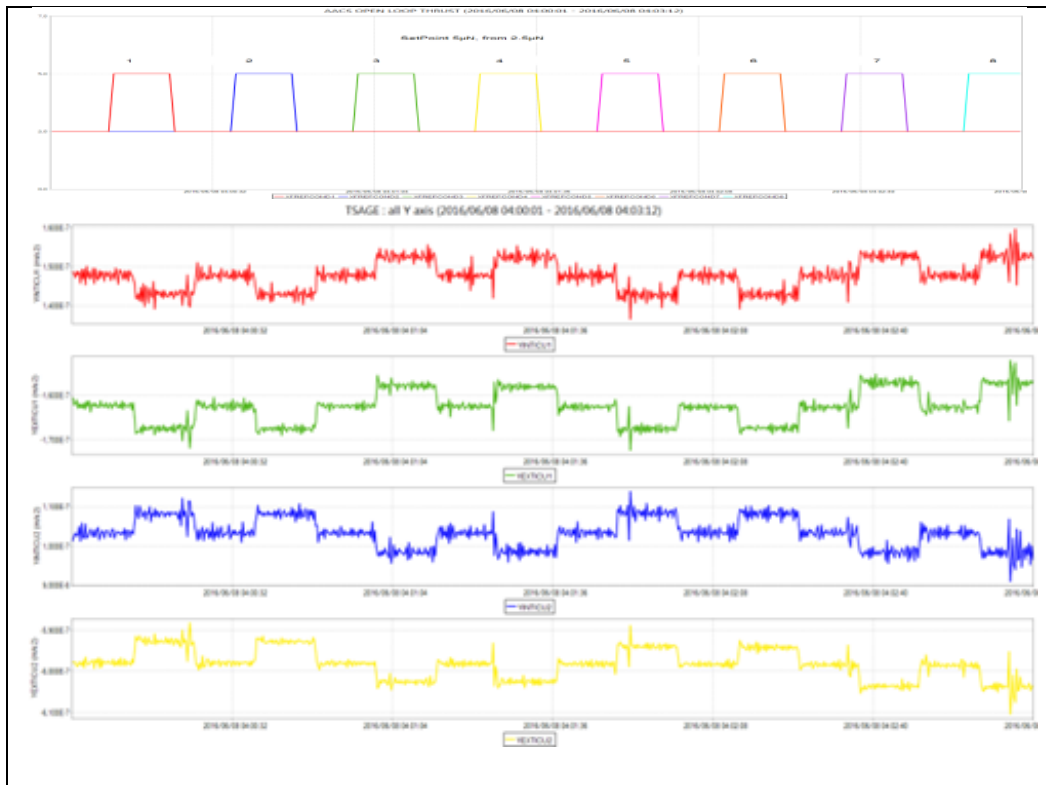


Figure 15 DFACS open loop thrust (set-point 5µN)

Figure 16 highlights with an example the dynamics of both CGPS and TSAGE. The blue line displays the set point of a thruster (4Hz telemetry from ECM). The red line (4Hz telemetry from TSAGE) is the resulting acceleration measured by the external mass of EP (the titanium TM) about Y axis. The green line is the MFS voltage.

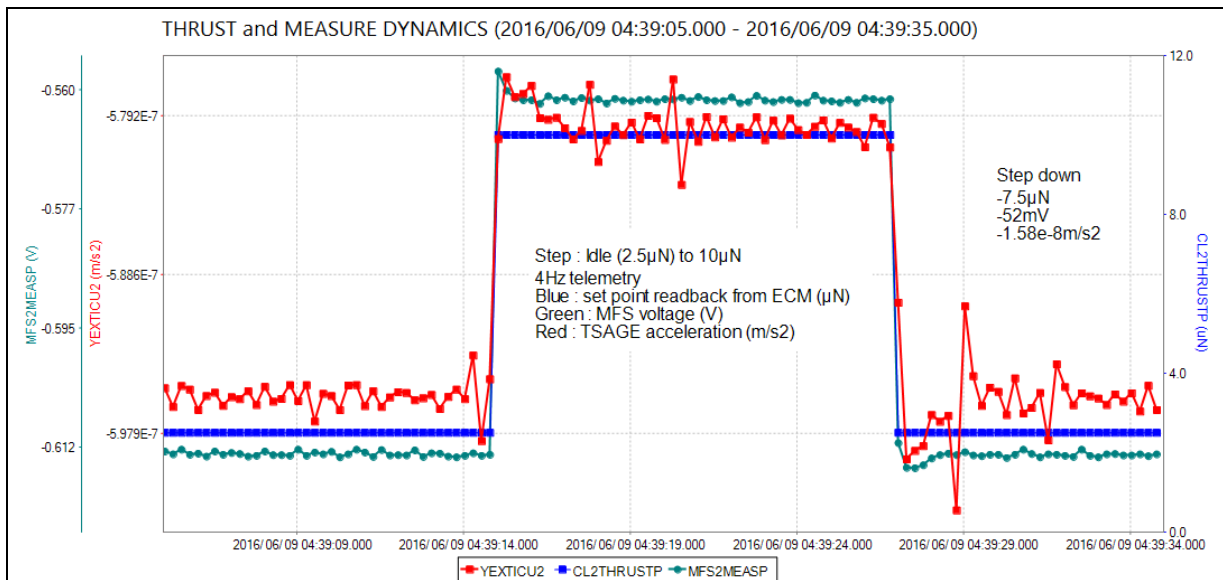


Figure 16 A step 2.5 to 10 µN, thruster setpoint and TSAGE measure

Even if some fine correction of synchronization should be made (the read-back from ECM has a 250ms delay while TSAGE measure is advanced of a fraction of 250ms), one can observe the rise and fall time. The response time of the chain (thruster+TM suspension) is consistent with predictions (250ms@63% for the thruster and 1.8Hz low pass filter for TSAGE). The green line (MFS voltage) confirms the amazing precision of the thruster’s control loop. For memory, such a step means a  $7.5\mu\text{N}/(g_0 \cdot \text{ISP}) \sim 15.3 \mu\text{grams}$  per second of gas flux ! In addition to dynamics

of both CGPS and TSAGE, the precision of the whole system is remarkable (rise/fall symmetry, etc.).

Figure 17 displays the 6 axis measurement of one TM (4Hz telemetry) when a step from idle ( $2.5\mu\text{N}$ ) to  $100\mu\text{N}$  is successively commanded to each one of the 8 thrusters. The linear acceleration lies on the left side of the graph while the right side presents the angular accelerations. Both thrust control loop and mass suspension loop have a slight overshoot, no surprise to find quite large overshoots on such an experiment. It is worth to notice the excellent behavior of TSAGE on angular axes.

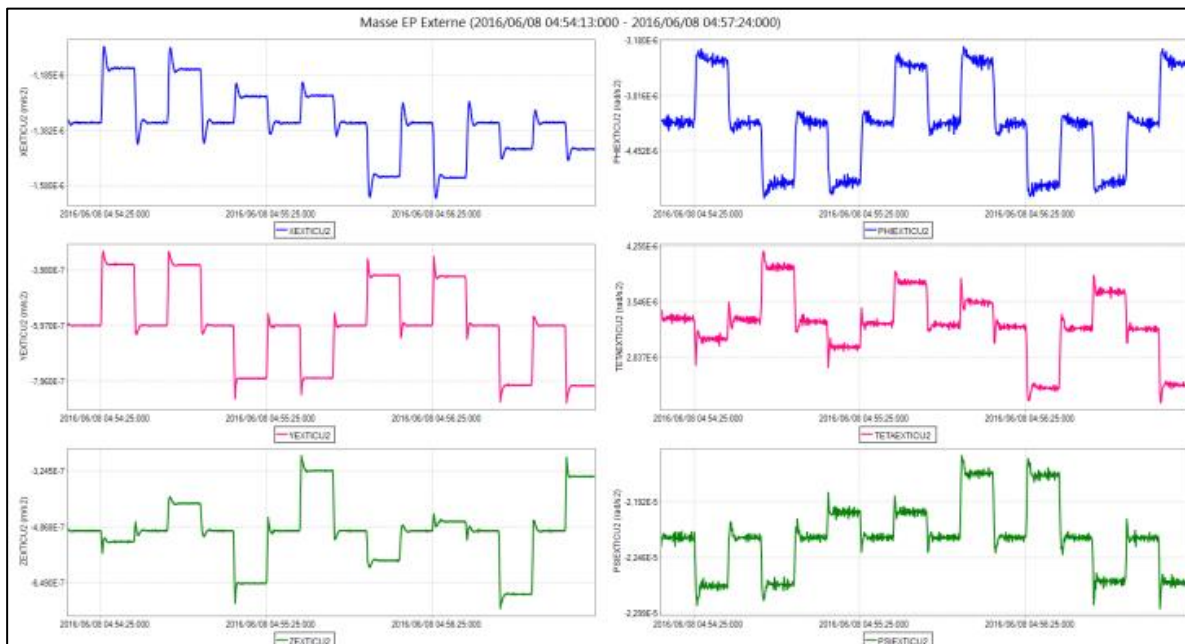


Figure 17 AACS open loop thrust, set-point  $100\mu\text{N}$ , 6 axis measure EPext (titanium TM)

As we have 4 TM, each one delivering signals like Figure 17, and we accurately know the locations and orientations of both the TM and the thrusters, we tried to estimate the ‘real’ 6 axes acceleration of the s/c. Our first idea was to consider TSAGE as a perfect accelerometer and to observe the real thrust. We failed to find consistent estimates. Actually we have significant cross axis coupling in TSAGE (except toward the most sensitive axis), specifically from linear to angular. Symmetrically, the observation the TM sensitivity  $6\times 6$  matrix considering the real acceleration as an input (given model of propulsion) was also a dead-end. The experiment involves too much parameters playing together. It’s useful to confirm a model but not to identify without ambiguity.

This experiment was first performed with the nominal propulsive configuration during in-flight testing and then with both the nominal and redundant configurations during dedicated end-of-life experiments. In both cases results show a linear evolution of the estimated thrust under-efficiency (see. Figure 18) with a scale factor of 75.9% for the nominal configuration and 87.7% for the redundant configuration. These scale factors confirm the efficiency previously observed with the gas consumption monitoring and the “tangential thrust” experiment. This may be caused by an imperfect calibration of the mass flow sensors scale factors ( $\mu\text{N}$  to Volt conversion).

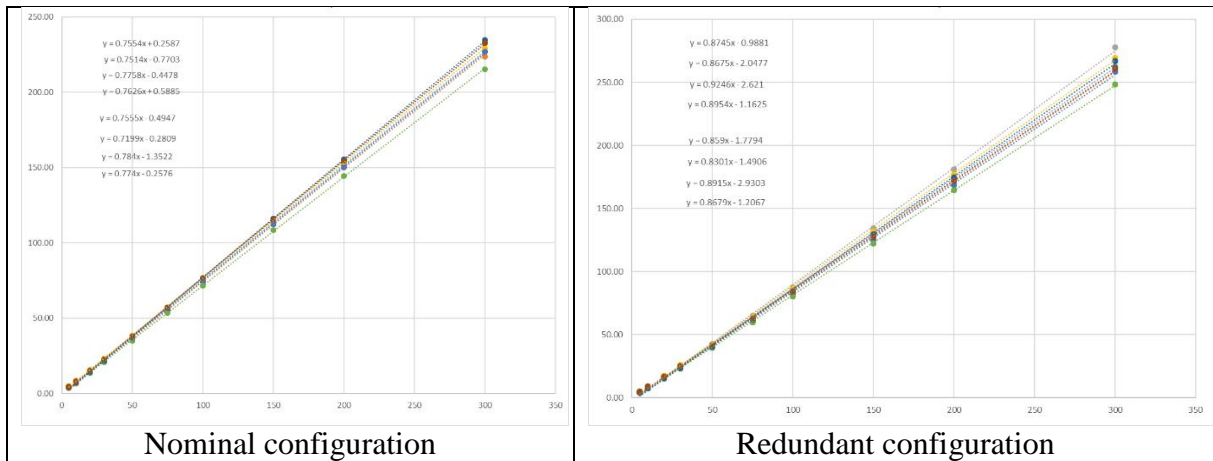


Figure 18 Estimated thrusts vs commanded thrusts ( $\mu N$ )

### End-of-Life Monitoring

In order to manage the uncertainties on the high pressure measurements, the scientific mission ended when the central estimation of the remaining gas in the tanks was 123g for Z+ and 142g for Z- (about 4 bar each). This low unbalance between both walls (compatible with the end-of-life uncertainty margins) after a 2-year mission was achieved through a constant monitoring of TSAGE biases. To vent the tanks, a last propulsive session was performed. Using the results of the “Increased Idle” experiment, the idle was set to 100 $\mu N$  to speed up the venting. As expected, the session was stopped after ~17 orbits by the CGPS’s failure detection system, inducing a retreat in safe hold mode. The consumption was consistent with the one observed during the experiment (6g/orbit/wall). A first analysis of the pressure measurements (see Figure 19 : two high pressure sensors and one low pressure sensor per wall) shows that the pressure regulators operated until 1.8 bars, far below the nominal operating domain (> 10 bars). Moreover, the thrusters perform very well with an inlet pressure lower than 1 bar (until 0.5bar).

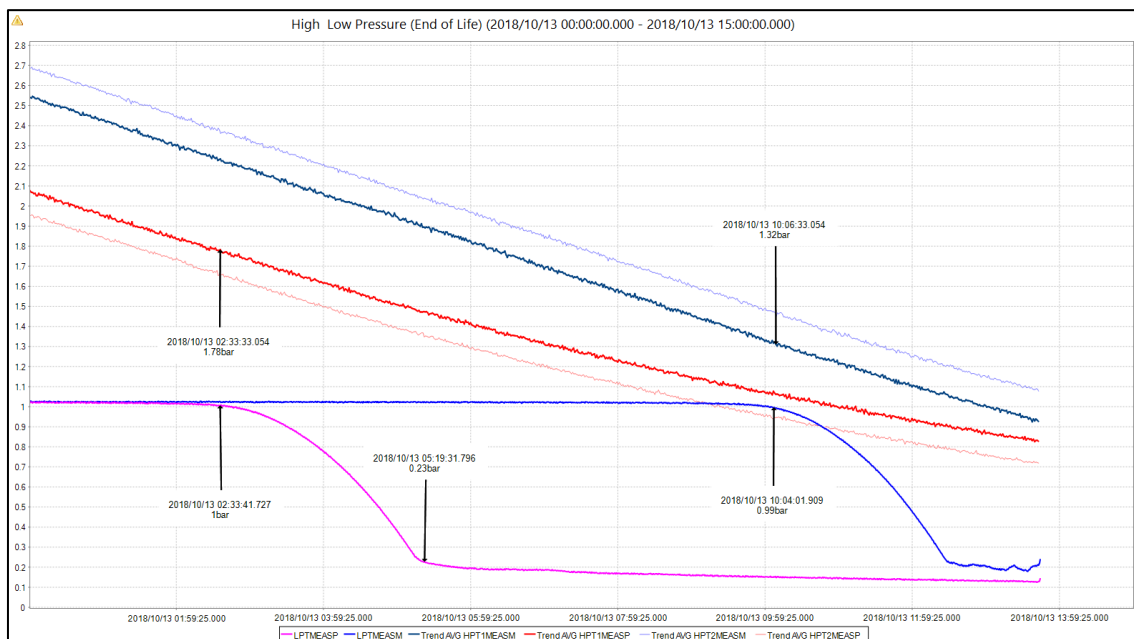


Figure 19 High (HP) and low (LP) pressure evolution during the gas venting session

## Collision avoidance management

In the early stage of the project, it has been decided that despite the low maneuverability of the satellite the collision avoidance had to be managed. Thus a specific strategy was developed using the available propulsive system to perform the avoidance manoeuvre ([6]).

The objective of the avoidance manoeuvre is to insure a sufficient radial separation with the incoming object. To achieve this separation, a tangential force has to be applied to the satellite. Geocentric mode was proven to be the most efficient guidance to generate a tangential force with the available configuration (which means an interruption of the scientific mission to rally this guidance). The force is commanded in open loop to the thrusters, in addition to the attitude control command (in a propulsive mode with drag-free off). A thrust budget study determined a maximal tangential thrust of  $360\mu\text{N}$ , which would generate a 100m radial separation in 12h, enough to mitigate the risk.

The tangential thrust is commanded on the Ysat axis for a maximum efficiency. Due to the geometrical configuration, a  $F_y=100\mu\text{N}$  implies a  $220\mu\text{N}$  cumulated thrust (shared on 2 MT per walls). Thus, a 12h avoidance manoeuvre would drink  $\sim 100\text{g}$  of Nitrogen ( $\sim 20\text{g}$  for attitude control and  $\sim 70\text{g}$  for the manoeuvre). This is equivalent to a 5-day low spin session (in addition to the consumption linked to a possible reschedule of the interrupted session).

Fortunately, no need of collision avoidance was detected, and this strategy was only applied during in-flight testing over a reduced duration.

## Deorbiting solution

Another issue to consider with a low maneuvering satellite is the deorbiting strategy. Indeed, Microscope had to respect the French Regulation on Space Operations (LOS). This regulation will officially start in 2020, but it is already applicable to CNES (which as the French Space Agency has to lead by example). The mission design had thus the obligation to guaranty the atmospheric re-entry of the satellite within 25 years.

At first, studies were conducted to analyze the feasibility of additional propulsive solutions, but the constraints for integration were incompatible with the satellite design: strong increase of inertias incompatible with the DFACS performances, thermal stability issues, need of attitude control during the thrust ... At this stage, an opportunity came by with an on-progress research concerning the development of a sail system (for antennas' purpose). Flight dynamics analysis allowed to determine the optimal size and orientation of the sail. Indeed, as it wasn't possible to guarantee a stable attitude during the all re-entry phase, the mean dragging surface necessary to insure a 25-years re-entry had to be attitude independent.

IDEAS (Innovative DEorbiting Aerobrake System) was installed on the +X side of the satellite (on the opposite side of the launcher interface). It includes 2 wings and inflatable mats, long of 4.54m each, and an inflation system. The +X wall was almost dedicated for IDEAS, so that it could be developed independently.

Figure 20 shows Microscope with IDEAS fully deployed. The left image is the design engineering model, and on the right is a radar image taken by the space observation radar TIRA (Fraunhofer Institute) during de-orbiting. In addition to the deployment monitoring at the Ground Control Center, the good consistency between the model and the image was a reassuring proof of the correct deployment of the system.

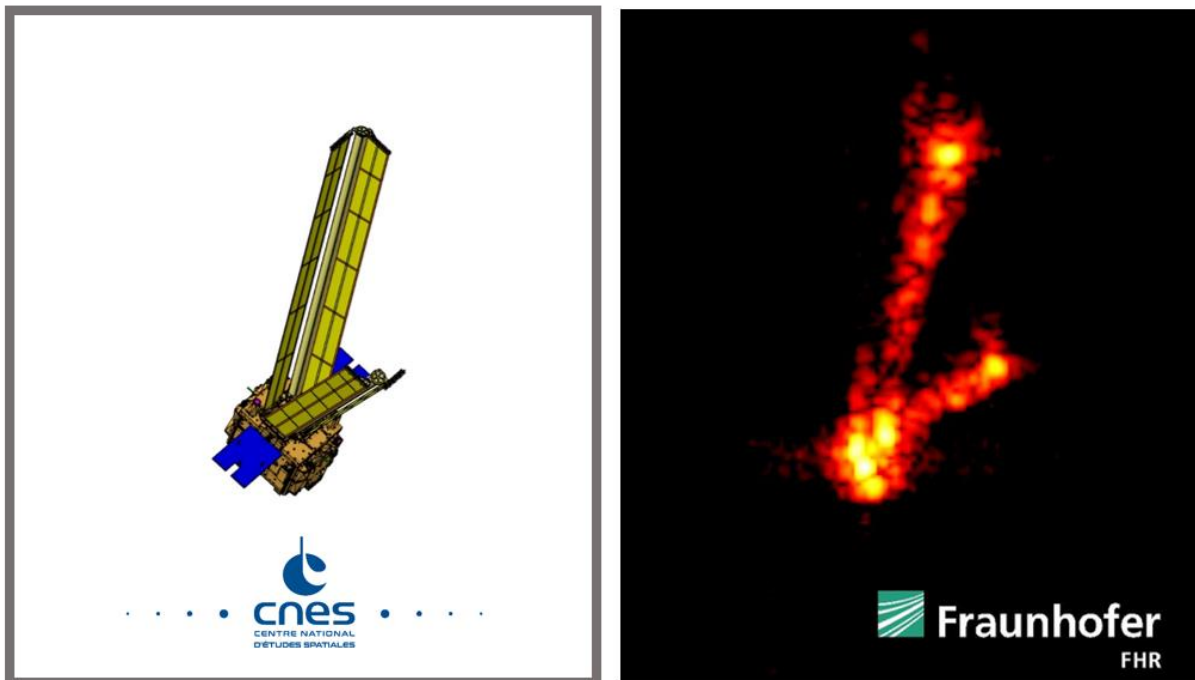


Figure 20 Microscope with IDEAS fully deployed : engineering model (left) and image by the radar TIRA (right) taken on October 17<sup>th</sup>

## Lessons Learned

### EP Testing

Concerning the scientific objective of the mission, the amount of collected data is limited by lifetime and then linked to the gas consumption. The commanded thrust was mainly due to torques. In a low solar activity period the magnetic perturbation is dominating for low orbits, and the SpinMax sessions generated a high gyroscopic torque due to inertia unbalance  $I_{xz}$ .

As explained in the “Architectural Choices” section, the classical AOCS design using reaction wheels and magneto-torquers (MTQ) was rejected due to micro-vibration and magnetic perturbations. However, even if such perturbations wouldn’t have been an issue, the use of MTQ would have only been possible with a linear driver instead of the usual pulse-width modulation. Indeed, due to the length of the scientific sessions, wheels unloading would have occurred within sessions, and a linear driver would have insured a smoother actuation law more compatible with the acceleration requirement than the usual on-off modulation.

Concerning the SpinMax sessions, if those had been foreseen during the mission design, even more attention would have been given to the satellite centering and inertia. The satellite center of mass and the TM location must be aligned with the spin axis to limit centrifugal force. Inertia tensor must be diagonal to limit the gyroscopic torque. A Center of Mass Trim Assembly (MTA) would have been particularly useful to adjust the center of mass and diagonalize the inertia tensor during the flight, thus probably reducing the consumption from 3.5g/orbit/wall to less than 1g/orbit/wall.

## Aeronomy

For Microscope, specifications for aeronomy (precise measurement of the drag accelerations for atmospheric modelling) were not considered in the design. Aeronomy is quite incompatible with the use of thrusters which inevitably perform a non-negligible force (even used only for attitude control). End-of-life aeronomy experiments were however conducted but with a non-optimal configuration. The satellite was set in a non-propulsive mode (no drag-free and coarse attitude control with MTQ), which implied to activate TSAGE only in full-range mode (to handle the acceleration levels). The poor attitude control, the angular accelerations and the cross axes coupling made them difficult to analyze.

If the aeronomy needs had been taken into account in the satellite design, a specific AOCS mode would have been studied with 3 reaction wheels (for the geocentric pointing) and magneto-torquers (for wheels unloading). Moreover, to avoid periodic wheels unloading (during determined on-orbit position slots), a continuous unloading would have been possible with a linear driver of the MTQs.

## Conclusion

Microscope is a great success in terms of DFACS architecture and performance. The association of the scientific accelerometer and the cold gas propulsion system proved to be perfectly suited to the mission requirements.

The general behavior of the cold gas propulsion system has been analyzed all along the mission, showing very satisfactory performance:

- The cold gas monitoring demonstrated that the consumption for a given guidance (from 0.6 g/orbit/wall up to 3.5 g/orbit/wall) is very stable, thus allowing a precise management of the mission scenario.
- An under-calibration of the thrusters (about -25% for the nominal set and -10% for the redundant set) was observed. However, this scale factor was easily compensated by the DFACS close loop.
- Thrusters were tested at heavy load ( $\sim 200\mu\text{N}$ ), showing that the dynamic performance (response time, noise) are not affected and the scale factor remains under 5%.
- Above all, all the thrusters were demonstrated perfectly operational until the end.

In short, CGPS gave full satisfaction for Microscope mission. This technology demonstrated both robustness and amazing performance.

Microscope was de-orbited on October 16<sup>th</sup> 2018, after a 2-year successful mission. Scientific analyses of the large amount of collected data are still on-going, and the first results are very promising ([7]).

Concerning the DFACS expertise, the analyses showed that the drag-free performance on Microscope is by far the finest ever achieved on low Earth orbit:  $<10^{-12} \text{ m/s}^2$  @Fep, three axes for up to 8 days.

## Acknowledgments

The authors would like to thank the whole MICROSCOPE project team for making this adventure possible. Special thanks go to our orbitography CECT partner David PASCAL, and to our AACS design partners Christelle PITTET, Florence GENIN, Maxime JOURNOT, Céline BELLET, Alain PEUS and Frédéric VIAUD.

## References

1. Prieur P., Liénart T., Rodrigues M., Denver T., Touboul P., Metris G., “Microscope mission: on-orbit assessment of the drag-free and attitude control system”, ISSFD-2017-038, *International Symposium on Space Flight Dynamics*, Matsuyama, Shikoku Island, Japan, 2017.
2. Liénart T., Bertuccio E., “Design, manufacturing and testing of the Cold Gas Propulsion System for CNES' Microscope spacecraft: lessons learnt”, AIAA 2017-4747, *53rd Joint Propulsion Conference*, Atlanta, GA, U.S.A., 2017.
3. Viaud F., André Y., Cipolla V., Liénart T., Pfaab K., Pouilloux B., Prieur P., “Evolution of the propulsion sub-system on CNES' Microscope satellite from FEEPS to Cold Gas and subsequent impacts on the platform”, *The 4S Symposium*, 2016
4. Wiktor P., “The design of a liquid helium propulsion system”, *Thesis report*, Stanford University, January, 1992
5. Delavault S., Prieur P., Liénart T., Robert A., Guidotti PY., “MICROSCOPE mission: drag-free and attitude control system expertise activities toward the scientific team”, *CEAS Space Journal*, 2017, 10.1007/s12567-018-0205-9.
6. Aitier E., “Microscope operations: collision avoidance and de-orbitation for a non-maneuvering satellite”, AIAA 2016-2451, *SpaceOps 2016 Conference*, Daejeon, Korea, 2016.
7. Touboul et al., “Microscope Mission: First Results of a Space Test of the Equivalence Principle”, PRL 119 231101 (2017), *Physical Review Letters*, December 8<sup>th</sup> 2017